SUPPLEMENTARY FIGURES AND LEGENDS

Supplementary Fig. S1 (related to Fig. 1). Lineage Tracing and FACS Sorting of Single Satellite Cells

(A) Satellite cells from *Pax7-CreER;R26R-tdTomato* mice were efficiently labeled with tdTomato after Tamoxifen induction. Single myofibers were isolated from EDL muscles of induced *Pax7-CreER;R26R-tdTomato* mice and stained for Pax7 and DAPI. Notably, all Pax7^{pos} satellite cells on the myofibers were marked with tdTomato (native fluorescence).

(B) Satellite cells differentiated only into myotubes in myofiber cultures under pro-myogenic culture conditions. Myofibers (n > 600) with resident satellite cells were isolated from *Pax7-CreER/R26R-tdTomato* EDL muscles and cultured for 12 days in pro-myogenic medium. Lineage marked satellite cell-derived multinucleated myotubes expressed tdTomato, but not Prdm16 or Perilipin A.

(C) Single satellite stem cells (ZsGreen^{pos}, Myf5-Cre-tdTomato^{neg}) and satellite myogenic progenitors (ZsGreen^{pos}, Myf5-Cre-tdTomato^{pos}) were sorted from *Pax7-ZsGreen;Myf5-Cre;R26R-tdTomato* mice and assayed for their potential for adipogenic differentiation. Shown are representative FACS profiles and the experimental scheme for clonal analysis of satellite cell-to-adipocyte differentiation.

(D) Satellite stem cells (ZsGreen^{pos}, Myf5-Cre-tdTomato^{neg}) and satellite myogenic progenitors (ZsGreen^{pos}, Myf5-Cre-tdTomato^{pos}) were faithfully isolated by FACS. Immunofluorescence staining reveals Pax7 expression in all FACS-sorted quiescent satellite cells (n > 300) and the absence or presence of tdTomato in satellite stem cells and satellite myogenic progenitors, respectively. Notably, immunofluorescence staining signals of Pax7 was collected from the infrared channel but pseudocolored into green in order to generate R/G/B-colored merge images.

(E) Single satellite cells were faithfully sorted by DAKO cytomation MoFlo high speed sorter. Shown are the experimental scheme and results of the fidelity test.

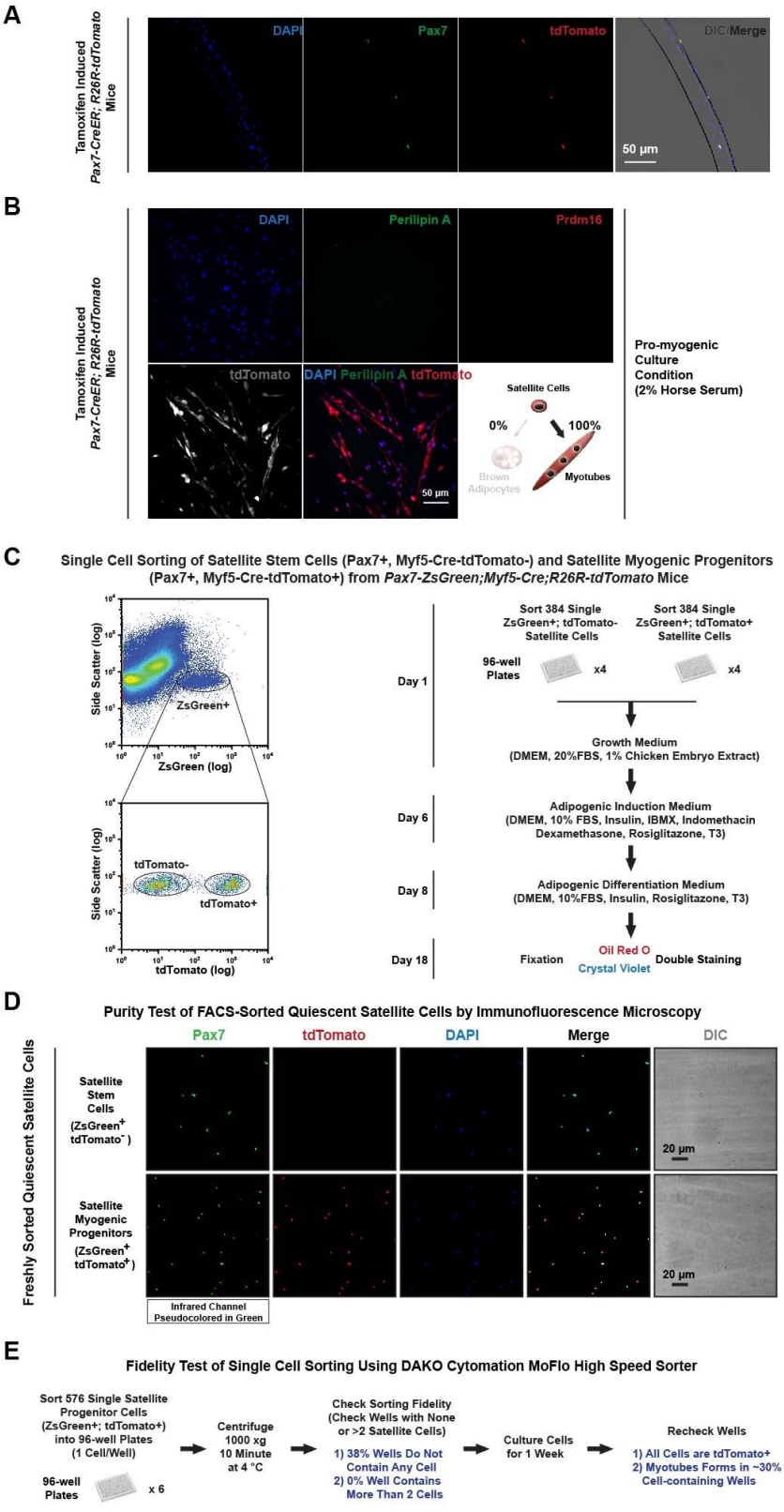

Supplementary Fig. S1

Supplementary Fig. S2 (related to Fig. 2). Inverse Gene Expression Patterns of miR-133 and Prdm16 in Myogenic and Brown Adipogenic Cells Revealed by RNA-Seq

(A) Representative FACS sorting profiles of isolating Sca-1^{pos}/Lineage^{neg} brown preadipocytes from interscapular BAT (iBAT) of new born mice.

(B-C) RNA-Seq revealed 580 mRNAs (B) and 88 microRNAs (C) that are differentially expressed in FACS-sorted satellite cells and brown preadipocytes. Shown are the hierarchical clustering and heat plots of these differentially expressed mRNAs and microRNAs. Some known markers for brown preadipocytes (red) and satellite cells (green) are labeled.

(D) A negative regulatory network illustrates putative repression of transcription factors enriched in brown preadipocyte (red) by satellite cell-enriched microRNAs (green). The microRNA target prediction was based on TargetScan 5.2. Notably, miR-133a and miR-133b target Prdm16 with high P_{ct} scores.

(E) Luciferase assays and qRT-PCR indicate miR-133 targets Prdm16 3'UTR and this repression depends on the predicted 8-nt seed sequence. miR-133 was over-expressed in C2C12 myoblasts together with *Renilla* luciferase reporter constructs containing either intact or mutated Prdm16 3'UTR. The repression of luciferase activity and expression by miR-133 was abolished by mutating the predicted 8-nt seed sequence. Notably, the luciferase activity and the luciferase mRNA level from the mutated *Renilla* luciferase reporter constructs were significantly higher than those of *Renilla* luciferase reporter constructs with intact seed sequences, which is presumably due to the presence of endogenous miR-133 in C2C12 myoblasts.

(F) qRT-PCR indicates that the expression levels of miR-133 and Prdm16 are inversely correlated in freshly FACS-sorted brown preadipocytes, total satellite cells, satellite stem cells, satellite myogenic progenitors as well as in cultured satellite cell-derived primary myoblasts.

Statistical analysis was done for pair-wise comparisons between brown preadipocytes and total satellite cells as well as between satellite stem cells and satellite myogenic progenitors.

Error bars: S.E.M., asterisk: significant pair-wise comparison by *t*-test, *: $p \leq 0.05$.

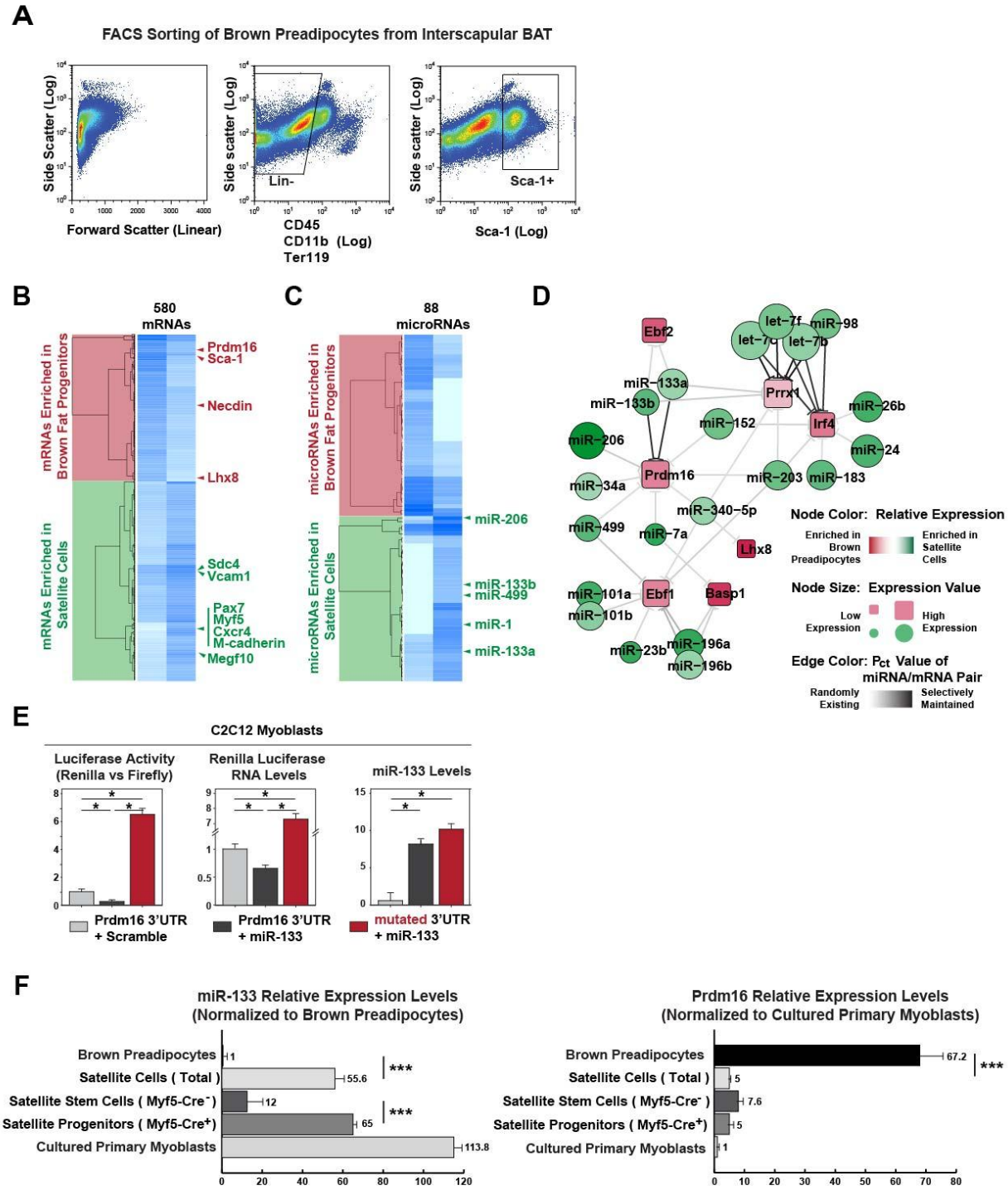

Supplementary Fig. S2

Supplementary Fig. S3 (related to Fig. 3). miR-133 Prevents Brown Adipose Determination in Myofiber-Associated Cells and Prdm16 is the Principal Target of miR-133 during Brown Adipose Determination

(A) The experimental scheme for miR-133 knockdown and over-expression in satellite cells from isolated single myofibers.

(B) Immunofluorescence indicates $Prdm16^{pos}$, $MyHC^{neg}$ brown adipocytes with visible oil droplets were markedly induced in myofiber cultures transfected with miR-133 inhibitors. Notably, no brown adipocyte was observed from myofiber cultures transfected with miR-133 mimetics. Without lineage tracing, the lineage origin(s) of brown adipocytes in the culture with miR-133 inhibitors was ambiguous. Nevertheless, miR-133 over-expression impaired the brown adipogenic commitment/differentiation whatsoever. DIC: differential interference contrast microscopy.

(C) The experimental scheme for determining whether miR-133 targets any brown adipose determinant other than Prdm16. miR-133 mimetics and/or over-expressing plasmid containing Prdm16 without 3'UTR (Prdm16 CDS) were transfected into C3H10T1/2 mesenchymal progenitors two weeks before adipogenic induction and differentiation. In theory, miR-133 mediated repression of Prdm16 and any potential BAT determinant upstream of Prdm16 can be rescued by over-expressing Prdm16 without its 3'UTR. By contrast, the putative repression of Prdm16 downstream determinants or Prdm16-independent determinants by miR-133 cannot be rescued by Prdm16 over-expression. Notably, C3H10T1/2 mesenchymal progenitors have been previously utilized to study functions of prostaglandin in brown adipose determination (Vegiopoulos et al., 2010), whereas brown preadipocytes are not suitable for this assay given their predetermined lineage fate and endogenous expression of miR-133 and Prdm16.

(D) Over-expression of miR-133 together with Prdm16 let to a comparable level of brown adipose differentiation as compared to Prdm16 overexpression alone. Immunofluorescence of Prdm16 and Perilipin A expression after adipogenic differentiation indicates that the brown adipose differentiation of C3H10T1/2 mesenchymal progenitors transfected with miR-133 mimetics can be rescued by concomitant over-expression of Prdm16. Oil Red O staining of differentiated progenitors under various conditions was shown on the upper left corner of each immunofluorescence panel.

(E) Immunoblots show expression levels of Prdm16, UCP1, PGC1α, Perilipin A and α-Tubulin expression in C3H10T1/2 mesenchymal progenitors differentiated under pro-adipogenic conditions as well as MyHC expression in progenitors differentiated under pro-myogenic conditions. A lane of whole-tissue lysate prepared from hindlimb muscles on left served as a positive control for pan-MyHC immunoblotting.

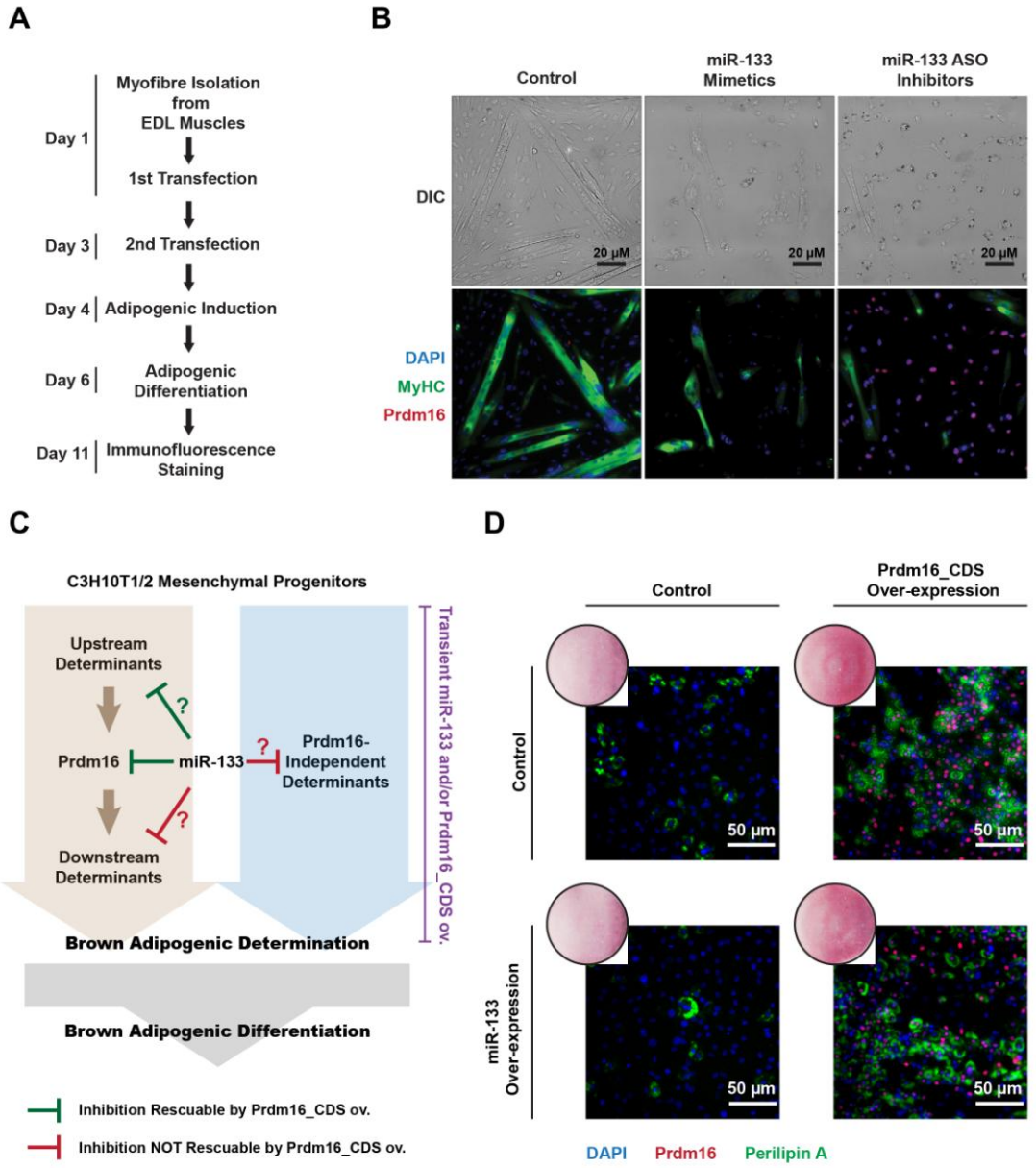

Supplementary Fig. S3

Supplementary Fig. S4 (related to Fig. 4). Antagonism of miR-133 Induces Brown Adipose Determination of Satellite Cells During Muscle Regeneration

(A) The experimental scheme for inducing brown adipocytes *in vivo* via miR-133 antagonism and data collection.

(B) Long-lasting effect of miR-133 antagomiR (ASO) *in vivo*. qRT-PCR indicates reduced expression of both *miR-133a* and *miR-133b* after 90 days of intramuscular miR-133 ASO administration. *Ucp1* mRNA was markedly induced in regenerating TA muscles by miR-133 ASO.

(C) Immunoblots reveals that BAT-specific UCP1 was reproducibly induced by miR-133 antagonism in regenerating muscles. Protein lysates were prepared from clean-dissected TA muscles without any visible fat tissue from three independent experiments. Notably, the UCP1 antibody (from Calbiochem) was different from the antibody utilized in immunoblotting shown in Fig. 4B (from Abcam), but revealed the same induction of UCP1 in response to miR-133 ASO. The comparable protein levels of tdTomato indicates that similar levels of satellite cell-dependent muscle regeneration underwent in TA muscles received control ASO or miR-133 ASO.

(D) Muscle regeneration, rather than Cardiotoxin, is required for miR-133 ASO induced brown adipose determination in muscle. qRT-PCR indicates decreased expression of both *miR-133a* and *miR-133b*, increased expression of *Ucp1* in miR-133 ASO treated TA muscles after 30 days of frozen injury. Notably, the expression of *miR-206* was not affected by miR-133 ASO.

(E) Haematoxylin & Eosin (H/E) staining reveals that drastically increased numbers of interstitial cells were present in regenerating TA muscles received miR-133 ASO as compared to those received control ASO at the same regeneration stage (30 days post Cardiotoxin injection).

(F) Oil Red O staining suggests adipocytes were present within the muscle interstitium in response to miR-133 ASO treatment. Shown are representative images of Oil Red O autofluorescence detected in Rhodamine channel within cross-sections of TA muscles received control- or miR-133 ASO during regeneration. Notably, Oil Red O autofluorescence was centered in muscle interstitium.

(G) Averaged counts of $UCP1^{pos}$ cells on each cross-section of TA muscles received control- or miR-133 ASO. $tdTomato^{pos}$ and $tdTomato^{neg}$ cells were separately counted. Given the typical size of TA muscles after CTX-induced regeneration, at least tens of thousands $UCP1^{pos}$ brown adipocytes were present in miR-133 ASO treated muscle.

(H) Averaged counts of $Prdm16^{pos}$ cells on each cross-section of TA muscles, received control- or miR-133 ASO. $tdTomato^{pos}$ and $tdTomato^{neg}$ cells were separately counted. Given the typical size of TA muscles after CTX-induced regeneration, at least tens of thousands $Prdm16^{pos}$ brown adipocytes and committed preadipocytes were present in miR-133 ASO treated muscle.

Error bars: S.E.M., asterisk: significant pair-wise comparison by *t*-test, *: $p \leq 0.05$, **: $p \leq 0.01$, ***: $p \leq 0.001$.

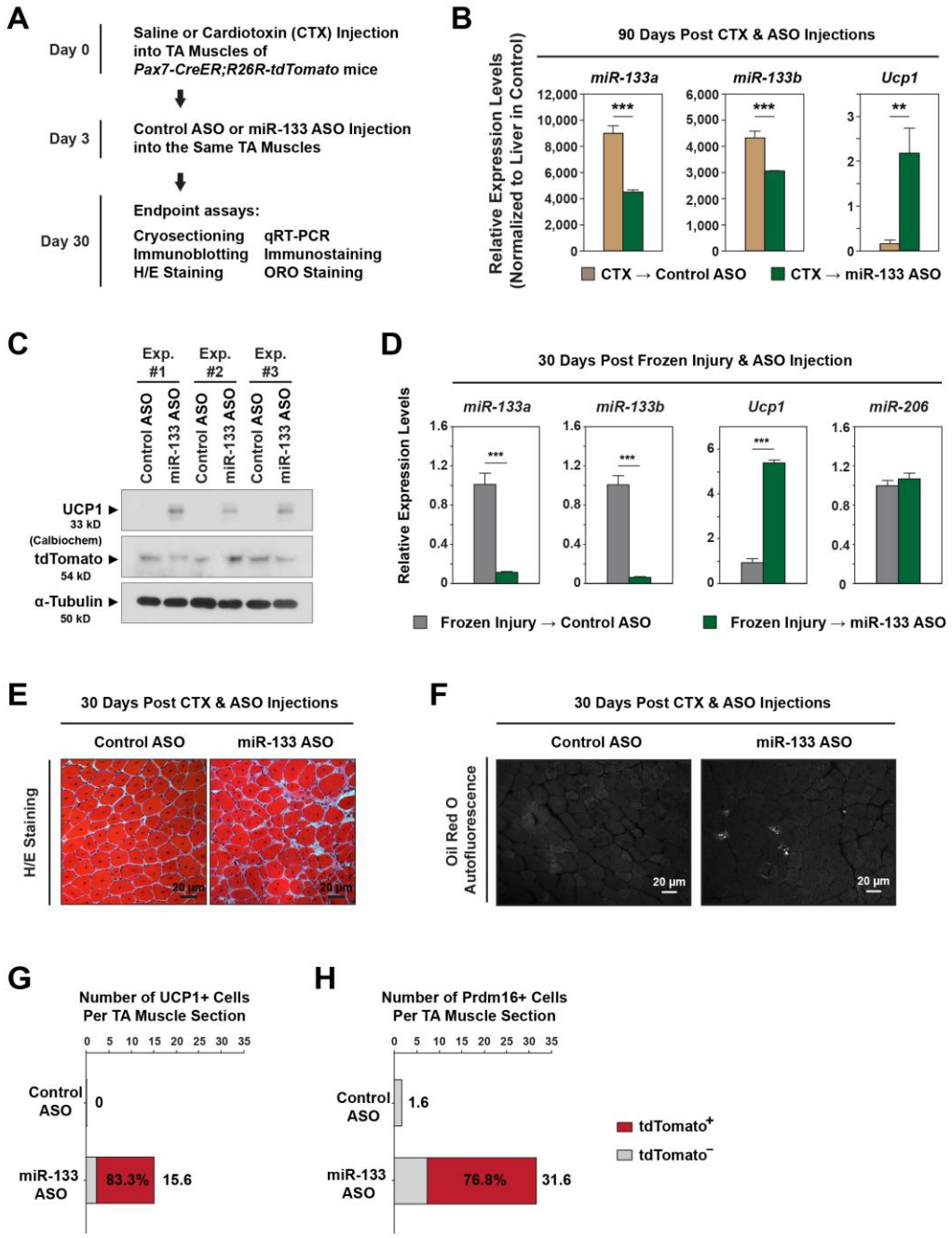

Supplementary Fig. S4

Supplementary Fig. S5 (related to Fig. 5). Brown Adipocytes Function Normally in Muscle Received miR-133 Antagonism during Regeneration

(A) High-resolution respirometry of contralateral soleus muscles in control- or miR-133 ASO treated mice. The control- or miR-133 ASO was always injected into the TA muscles of right hindlimbs. Here, the soleus muscles of the left (contralateral) hindlimbs served as a negative control for brown adipocyte-mediated uncoupled respiration as well as a site to test for a putative "systematic training effect" of miR-133 ASO on differentiated muscle cells. Notably, nonphosphorylating ("leak" uncoupled) respiration was comparable in contralateral soleus muscles from both control- and miR-133 ASO treated mice. In addition, there was no difference in terms of ETF or maximal oxidative phosphorylation capacity (P_{I+II}) between contralateral soleus muscles of two treatment groups.

(B) Representative [^{18}F]-FDG microPET/CT images of control ASO treated mice depict comparable levels of glucose/FDG uptake after acute CL316,243 treatment in the ASO treated TA muscle compared to the contralateral non-treated TA muscle. Dashed lines denote the levels for transverse and saggital cross-sections. The position of miR-133 ASO treated TA muscle was demarcated by dots on these cross-sections.

(C) qRT-PCR reveals the expression levels of acute inflammation markers (*IL-1b*, *TNF-a*) were comparable in control- or miR-133 ASO treated TA muscles in mice fed with either RD or HFD. Notably, *IL-1b* and *TNF-a* levels were measured at two months post cardiotoxin induced muscle injury, when the treated TA muscles had shown acute inflammation during the early muscle regeneration stage.

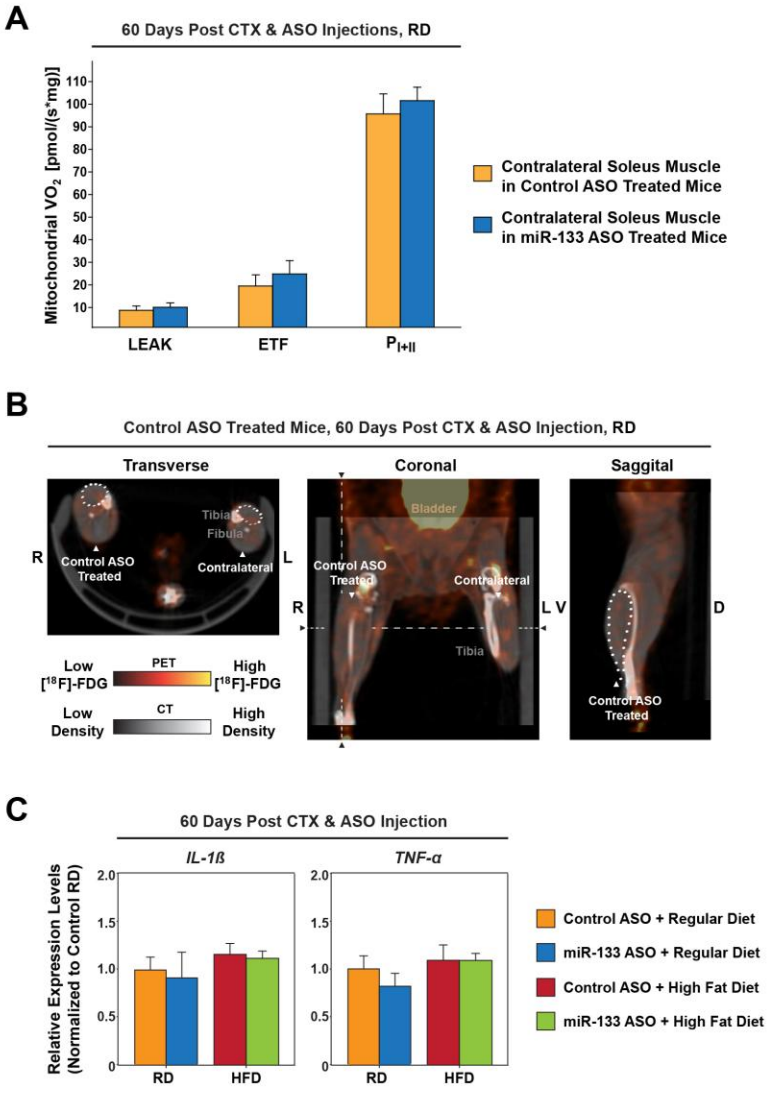

Supplementary Fig. S5

Supplementary Fig. S6 (related to Fig. 6). Antagonism of miR-133 During Muscle Regeneration Led to Reduced Adiposity and Ameliorated High Fat Diet-Induced Inflammation in White Adipose Tissue and Liver Steatosis

(A) miR-133 ASO treatment reduced adiposity. Weight of white fat depots showed less adiposity of miR-133 ASO treated mice fed either a regular diet (RD) or a high fat diet (HFD). Weight of interscapular brown fat depots and treated TA muscles were also determined.

(B) Indirect calorimetry reveals that mice received miR-133 ASO treatment during TA muscle regeneration recorded higher energy expenditure than the control mice (n=5 per group) during the light cycle (fed the HFD). Values of total energy expenditure were plotted without normalization to lean body mass.

(C) Physical activities measured during indirect calorimetry (C) reveal comparable physical activities within the light and dark cycles between control- and miR-133 ASO treated mice (fed the HFD). Physical activities are presented as arithmetic means of beam breaking events at X-, Y- and Z-dimensions.

(D) Resting respiratory exchange ratios (RER) measured at 22°C by indirect calorimetry. Notably, miR-133 ASO treatment in RD group reduced RER, whereas miR-133 ASO treatment in HFD group prevented the conspicuously low RER seen in control mice.

(E) Food intake measured within 24 hours for C57BL/6 mice (18-week old) fed with RD or HFD at 2 months after treatment of control- or miR-133 ASO during muscle regeneration. Pair-wise comparisons were performed by *t*-test. n.s.: not significant ($p > 0.05$).

(F) IPGTT tests for C57BL/6 mice received either control- or miR-133 ASO treatment (fed the HFD; n=6 per group).

(G) Representative images of Haematoxylin & Eosin staining of cross-sections of inguinal WAT (igWAT), epididymal WAT (epiWAT), interscapular BAT (iBAT) and liver from C57BL/6 mice fed with a HFD and 4 months after treatment of control- or miR-133 ASO. Arrowheads denote infiltrated inflammatory cells evidently present in epiWAT of control mice, whose number was reduced in epiWAT of miR-133 ASO treated mice.

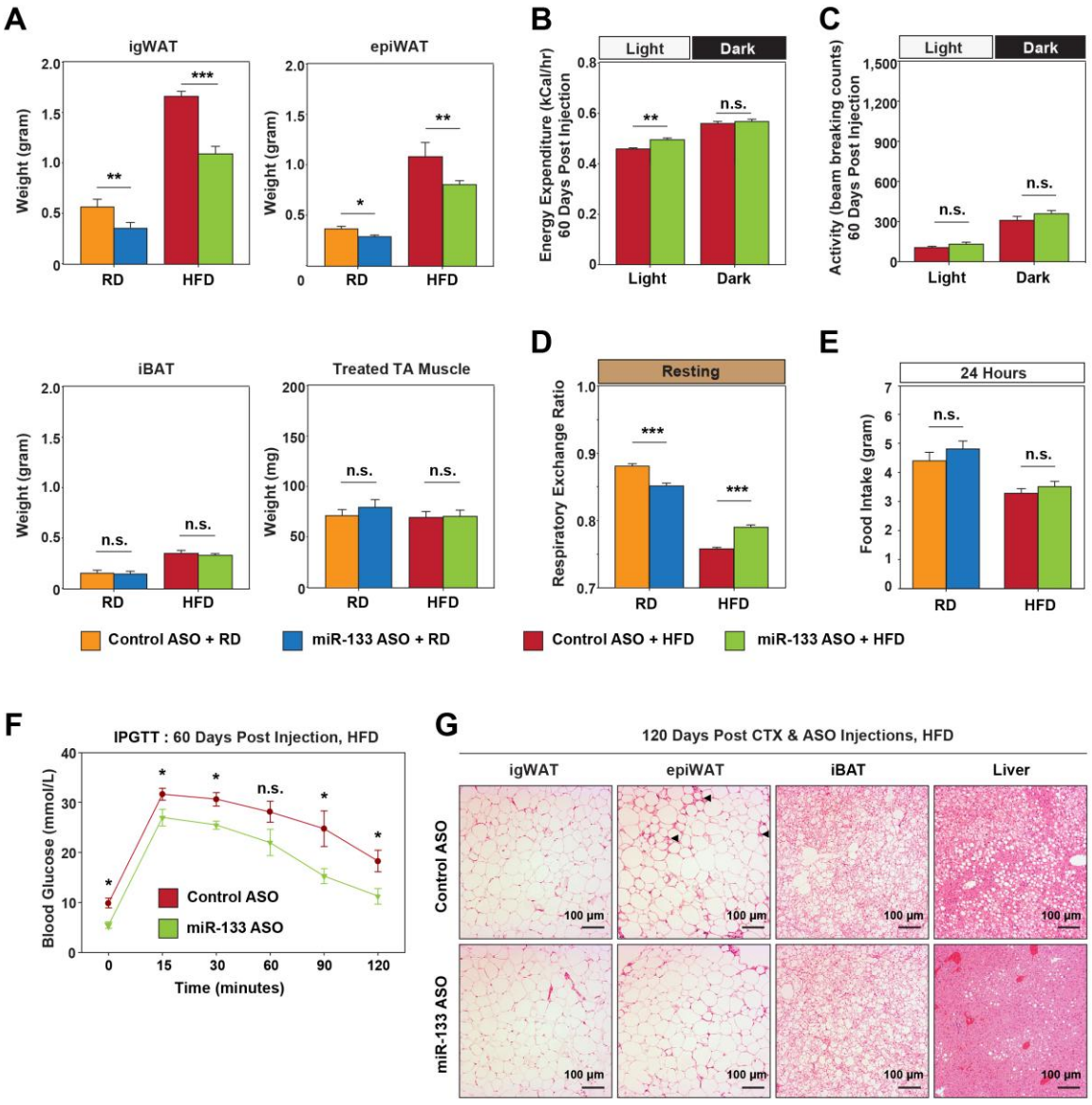

Supplementary Fig. S6

SUPPLEMENTARY EXPERIMENTAL PROCEDURES

Animals

All animal procedures conform with the Canadian Council on Animal Care's Guide to the Care and Use of Experimental Animals, the Animals for Research Act, and were approved by the Animal Care Committee at University of Ottawa. Individual caged C57BL/6 male mice were purchased from Charles River. All other mice were maintained on a C57BL/6 background. Following mice were used in this study: *Pax7-CreER/+* mice (Nishijo et al., 2009) (a kindly gift from Dr. Charles Keller), *Gt(ROSA)26Sortm9(CAG-tdTomato)*^{Hze} mice (Jackson laboratory), Pax7-ZsGreen mice (Bosnakovski et al., 2008) (a kindly gift from Dr. Michael Kyba), Myf5-Cre/+ mice (Tallquist et al., 2000). To induce Cre expression from *Pax7-CreER* locus, 200 µL Tamoxifen/corn oil solution (20 mg/mL) was intraperitoneally injected into 6-week-old mice for consecutive 5 days. For cold exposure, C57BL/6 mice and *Pax7-CreER/R26R-tdTomato* mice were gradually accustomized to decreasing temperature in 3 days and maintained at 4°C for one week with food and water *ad libitum.*

RNA-Seq and smRNA-Seq analyses and bioinformatic prediction of microRNA targets

RNA-Seq libraries were generated by Ovation® RNA-Seq System (NuGEN). Small RNA libraries were constructed with barcoded adaptors following Illumina's recommendations for multiplexing small RNA sequencing. RNA sequencing was performed on Solexa GIIx station. Expression values of mRNA were called by TopHat/Cufflink pipeline. Expression values of microRNAs were calculated by a Perl code designed to associate aligned reads with microRNA annotations within the genome (miRBase ver.16, http://www.mirbase.org). TargetScan (ver. 5.2), was used to predict microRNA target sites in 3'UTRs. A negative regulatory network was built by Cytoscape (ver. 6.0).

Myofiber isolation and culture

Single myofibers were isolated from *extensor digitorum longus* (EDL) muscles of 8~10 weeks old mice as previously described (Kuang et al., 2007). Myofibers were cultured in Dulbecco's modified eagle medium (DMEM) supplemented with 4.5 g/L glucose, L-glutamine, sodium pyruvate, 20% FBS and 1% chicken embryo extract without Penicillin or Streptomycin.

Fluorescence activated cell sorting (FACS)

FACS analysis and sorting were performed on a MoFlo High Speed Sorter (DAKO-Cytomation) equipped with 488 nm, 633 nm and UV lasers. Primary brown preadipocytes were FACS-sorted from interscapular BAT of neonatal mice as previously described (Seale et al., 2008). Primary white preadipocytes were FACS-sorted from subcutaneous (inguinal) white fat depots of 10-week-old mice as previously described (Rodeheffer et al., 2008). FlowJo version 8.7 software suites were used to analyze FACS data.

Cell culture

C3H10T1/2 mesenchymal progenitors were purchased from ATCC and cultured following manufacturer's recommendations. Adipocyte differentiation was performed as previously described (Seale et al., 2008). For myogenic differentiation, cells were cultured in DMEM supplemented with 2% horse serum.

Transfection of microRNA precursors and inhibitors

50 nM miR-133a and miR-133b Pre-miR™ Precursor (Ambion), 50 nM miR-133a/miR-133b PNA inhibitors (Panagene, Korea) were transfected into target cells by Lipofectamine RNAiMax reagent (Invitrogen) following manufacturers' recommendations.

High-resolution respirometry

Surgically extracted tibialis anterior (TA) and contralateral soleus (SOL) muscles were immediately placed in ice-cold biopsy preservation solution (BIOPS) containing 10 mM CaK_2EGTA buffer, 7.23 mM K_2EGTA buffer, 0.1 µM free calcium, 20 mM imidazole, 20 mM taurine, 50 mM 2-(N-Morpholino)ethanesulfonic acid hydrate (K-MES), 0.5 mM dithiothreitol (DTT), 6.56 mM $MgCl_2 \cdot 6H_2O$, 5.77 mM ATP, and 15 mM phosphocreatine (pH 7.1). The TA muscle was cut longitudinally into 4 equal parts, 2 of which were assessed by respirometry as intact cells and 2 after chemical permeabilization of the sarcolemma. The SOL muscle was cut in half longitudinally and both sections were permeabilized before respirometry. Prior to permeabilization muscle samples were gently dissected with two pairs of sharp forceps, achieving a high degree of fibre separation verified microscopically. Chemical permeabilization was achieved by incubation of the fibres with saponin (50 µg/mL) in 2 mL of BIOPS for 30 minutes at 4°C (Gnaiger, 2009a). Permeabilized samples were then rinsed with a mitochondrial respiration medium (MiR05) containing 0.5 mM EGTA, 3 mM $MgCl_2 \bullet 6H_2O$, 60 mM K-lactobionate, 20 mM taurine, 10 mM KH_2P0_4, 20 mM HEPES, 110 mM sucrose, and 1 g/L bovine serum albumin (pH 7.1).

Mitochondrial respiration

Muscle bundles (both intact TA, and permeabilized TA and SOL) were blotted and measured for wet weight in a balance controlled for constant relative humidity, providing hydration consistency and stability of weight measurements. Each sample was then placed into a single chamber of the high-resolution Oroboros Oxygraph-2k (Oroboros, Innsbruck, Austria) containing MiR05 solution and measured at 37°C. The Oxygraph is a two-chamber titration-injection respirometer with an oxygen detection limit of up to 0.5 $pmol \cdot sec^{-1} \cdot mL^{-1}$. Standardized instrumental calibrations were performed to correct for back-diffusion of oxygen into the

chamber from the various components, leak from the exterior, and sensor oxygen consumption. Oxygen flux was resolved by software allowing nonlinear changes in the negative time derivative of the oxygen concentration signal (Oxygraph 2k, Oroboros, Innsbruck, Austria).

Respiratory titration protocol

Intact cells: Uncoupled respiration was induced with the addition of malate (2 mM) and octanoyl carnitine (0.2 mM). This state represents the oxygen consumption of an unaltered and intact electron transport system (ETS) without the exogenous provision of adenylates. In the L_N state, the chemiosmotic gradient is at maximum and oxygen flux represents proton leak, slip, and cation cycling in muscle (Pesta and Gnaiger, 2011) and maximal respiration in BAT induced by fatty acids (Matthias *et al.* 2000). Further uncoupling of the ETS in muscle cells was assessed with the proton ionophore, carbonyl cyanide p-(trifluoromethoxy) phenylhydrazone (FCCP; 0.7 μM per titration up to concentrations ranging from 2.5–4 μM) to achieve a maximal uncoupling response.

Permeabilized cells: Uncoupled respiration in the absence of adenylates (L_N) was induced with the addition of malate (2 mM) and octanoyl carnitine (0.2 mM). Lipid oxidative phosphorylation capacity (P_{ETF}) and maximal electron flow through electron transferring-flavoprotein (ETF) was determined following the addition of ADP (5 mM). ETF is located on the matrix face of the inner mitochondrial membrane and supplies electrons from β-oxidation to coenzyme Q. The ETF linked transfer of electrons requires the metabolism of acetyl-CoA, requiring the addition of malate in order to facilitate convergent electron flow into the Q-junction from both CI and ETF allowing β-oxidation to proceed in permeabilized cells. The contribution of electron flow through CI is far below capacity and hence the rate limiting metabolic pathway is electron transport through ETF such that malate + octanoyl carnitine + ADP stimulated respiration is

representative of, rather than specific to, electron capacity through ETF (Gnaiger, 2009b; Pesta and Gnaiger, 2011; Pesta et al., 2011; Saks et al., 1998). Maximal NADH dehydrogenase (Complex I-specific) state-3 respiratory capacity (P_{CI}) was induced with glutamate (10 mM), which inhibits electron transport through ETF, isolating the transport of electrons through CI (Saks et al., 1998). Maximal mitochondrial state-3 respiration and oxidative phosphorylation capacity (P) was induced with the addition of succinate (10 mM) through succinate dehydrogenase, (complex II), and represents the mitochondrial capacity to catalyze a sequential set of Redox reactions primarily coupled to the production of ATP via ATP synthase. Convergent electron input to CI and CII, elicits higher respiratory values compared to the isolated respiration of either CI (pyruvate + malate or glutamate + malate) or CII (succinate + rotenone) (Gnaiger, 2009b) and accordingly is the physiologically relevant to the study of maximal coupled mitochondrial respiration. Oligomycin (1 μM) was then added to inhibit ATP synthase demonstrating oligomycin-induced leak respiration (L_{Omy}). Finally, Antimycin A (2.5 μM) was added to terminate respiration by inhibiting cytochrome bc_1 complex, allowing for the determination of residual oxygen consumption in the oxygraph chamber. Experiments were carried out in a hyperoxygenated environment (chamber oxygen concentration maintained above 300 nmol/ml) to prevent potential limitations in oxygen diffusion at high cell respiration rates. Finally, provision of the Redox substrates ascorbate (2 mM) and N,N,N',N'-tetramethyl-1,4-benzenediamine, dihydrochloride (TMPD, 5 mM) allowed for assessment of the isolated activity of cytochrome c oxidase (COX), the terminal respiratory chain complex that catalyzes the reduction of oxygen to water at the cytochrome aa3 subunit. Auto-oxidation of TMPD was corrected for by addition of sodium azide (100 mM). In permeabilized cell experiments, the oxygraph chambers were hyperoxynated (oxygen concentration above 300 nmol/L) to prevent

potential oxygen diffusion limitation.

Plasmid construction

A 293 bp fragment of Prdm16 3' UTR region, containing the miR-133 target site, was amplified from genomic DNA by PCR (sense primer: 5'-ACTCGAGTTCTCTGCTTGGATGGGCT-3'; antisense primer: 5'- AGCGGCCGCGACACAGGGGTATTTGGCA-3'). To generate the psiCheck2-Prdm16_wtUTR, amplified Prdm16 3'UTR fragment was cloned into XhoI/NotI site on psiCheck2 plasmid (Promega). To generate the psiCheck2-Prdm16_mutUTR, a site-directed mutagenesis PCR was performed on the psiCheck2-Prdm16_wtUTR template with Phusion® Site-Directed Mutagenesis Kit (Thermo Scientific;

forward primer: 5'-pGCCCCCGTGTGATAAGGTTGTGTGCTGTGTG-3';

revise primer:5'-pCGTTTTCACTACATACTTATATTAACATCATTTCTTCAGAATAAGTTGTCC-3'). For lentiviral overexpression of miR-133, a 619 bp region including the miR-133a hairpin precursor sequence was amplified from genomic DNA by PCR

(forward primer: 5'-AGAATTCTGAGCTGCAAGAACAGCAGTGT-3';

reverse primer: 5'-AGCGGCCGCTCCCATCATGTTTTTAGGTGAGTTTTTG-3'). The amplified sequence was cloned into EcoRI/NotI sites of pCDH-CMV-MCS-EF1-Puro plasmid (System Biosciences).

Luciferase assays

For miR-133 targeting assays, HEK293T cells were co-transfected with combinations of psiCheck2-Prdm16_wtUTR plasmid with Pre-miR™ Negative Control #1 Precursor (Ambion), or psiCheck2-Prdm16_wtUTR plasmid with miR-133a Pre-miR™ Precursor (Ambion), or psiCheck2-Prdm16_mutUTR plasmid with miR-133a Pre-miR™ Precursor.

Immunofluorescence staining

The following antibodies and dilutions were used: anti-MyHC antibody (MF20, Developmental Studies Hybridoma Bank), 1:20 dilution; anti-Prdm16 antibody (generated in Dr. Patrick Seale's laboratory), 1:1,000 dilution; anti-Perilipin A antibody (Vala Sciences), 1: 500 dilution; anti-Ucp1 antibody (Calbiochem), 1:200 dilution; anti-Laminin B2 antibody (Upstate), 1:500 dilution.

Immunoblotting

The following antibodies and dilutions were used: anti-Prdm16 antibody (generated in Dr. Patrick Seale's laboratory), 1:5,000 dilution; anti-Perilipin A antibody (Vala Sciences), 1:5,000 dilution; anti-Ucp1 antibody (Ab10983, Abcam), 1:1,000 dilution (Fig.s 4B, 5A); anti-Ucp1 antibody (Calbiochem), 1:1,000 dilution (Fig.s S4C); anti-Ucp3 antibody (Ab3477, Abcam), 1:1,000 dilution; anti-Pgc1α antibody (Abcam), 1:1,000 dilution; anti-pan myosin heavy chain (MyHC) antibody (Developmental Studies Hybridoma Bank), 1:500; anti-DsRed (tdTomato) antibody (Ablab), 1:500; anti-α-Tubulin antibody (Sigma-Aldrich), 1:10,000 dilution.

Immunohistochemistry (IHC)

Paraffin embedded tissue sections of TA muscles, inguinal white fat depots (igWAT) and epididymal white fat depots (epiWAT) were deparaffinized in CitriSolv. After rehydration, tissue sections were boiled in 0.01M citrate buffer (1.8 mM citric acid, 8.2 mM sodium citrate, pH 6.0) for 16 minutes. Endogenous peroxidase activity was neutralized by 0.3% H_2O_2 in 70% methanol. Anti-Ucp1 antibody (Calbiochem) was 1:200 diluted and incubated with tissues sections overnight. IHC signals were developed by Vectastain ABC kit.

Quantitative reverse transcription PCR (RT-qPCR)

Total RNA was extracted from cells by TRIzol or Arcturus® PicoPure® RNA Isolation Kit (Applied Biosystems) following manufactures' recommendations. For RT-qPCR of mRNAs,

total RNAs were reverse transcribed into cDNAs by SuperScript III (Invitrogen) and a mixture of oligodT_{18-20} primers and random hexamers. microRNA RT-qPCRs were performed as previously described (Shi and Chiang, 2005). Primer sequences used in RT-qPCR are provided in Supplementary Table S3A. Relative expression ratios were calculated by REST2009 (Qiagen).

SUPPLEMENTARY REFERENCES

Bosnakovski, D., Xu, Z., Li, W., Thet, S., Cleaver, O., Perlingeiro, R.C., and Kyba, M. (2008). Prospective isolation of skeletal muscle stem cells with a Pax7 reporter. Stem Cells *26*, 3194-3204.

Gnaiger, E. (2009a). Capacity of oxidative phosphorylation in human skeletal muscle: new perspectives of mitochondrial physiology. Int J Biochem Cell Biol *41*, 1837-1845.

Gnaiger, E. (2009b). Capacity of oxidative phosphorylation in human skeletal muscle: new perspectives of mitochondrial physiology. Int J Biochem Cell Biol *41*, 1837-1845.

Kuang, S., Kuroda, K., Le Grand, F., and Rudnicki, M.A. (2007). Asymmetric self-renewal and commitment of satellite stem cells in muscle. Cell *129*, 999-1010.

Nishijo, K., Hosoyama, T., Bjornson, C.R., Schaffer, B.S., Prajapati, S.I., Bahadur, A.N., Hansen, M.S., Blandford, M.C., McCleish, A.T., Rubin, B.P., *et al.* (2009). Biomarker system for studying muscle, stem cells, and cancer in vivo. Faseb J *23*, 2681-2690.

Pesta, D., and Gnaiger, E. (2011). High-Resolution Respirometry. OXPHOS Protocols for Human Cell Cultures and Permeabilized Fibres from Small Biopsies of Human Muscle. Mitochondrial Bioenergetics: Methods and Protocols *810*, 25-58.

Pesta, D., Hoppel, F., Macek, C., Messner, H., Faulhaber, M., Kobel, C., Parson, W., Burtscher, M., Schocke, M., and Gnaiger, E. (2011). Similar qualitative and quantitative changes of mitochondrial respiration following strength and endurance training in normoxia and hypoxia in sedentary humans. Am J Physiol Regul Integr Comp Physiol *301*, R1078-1087.

Rodeheffer, M.S., Birsoy, K., and Friedman, J.M. (2008). Identification of white adipocyte progenitor cells in vivo. Cell *135*, 240-249.

Saks, V.A., Veksler, V.I., Kuznetsov, A.V., Kay, L., Sikk, P., Tiivel, T., Tranqui, L., Olivares, J., Winkler, K., Wiedemann, F., *et al.* (1998). Permeabilized cell and skinned fiber techniques in studies of mitochondrial function in vivo. Mol Cell Biochem *184*, 81-100.

Seale, P., Bjork, B., Yang, W., Kajimura, S., Chin, S., Kuang, S., Scime, A., Devarakonda, S., Conroe, H.M., Erdjument-Bromage, H., *et al.* (2008). PRDM16 controls a brown fat/skeletal muscle switch. Nature *454*, 961-967.

Shi, R., and Chiang, V.L. (2005). Facile means for quantifying microRNA expression by real-time PCR. Biotechniques *39*, 519-525.

Tallquist, M.D., Weismann, K.E., Hellstrom, M., and Soriano, P. (2000). Early myotome specification regulates PDGFA expression and axial skeleton development. Development *127*, 5059-5070.

Vegiopoulos, A., Muller-Decker, K., Strzoda, D., Schmitt, I., Chichelnitskiy, E., Ostertag, A., Berriel Diaz, M., Rozman, J., Hrabe de Angelis, M., Nusing, R.M., *et al.* (2010). Cyclooxygenase-2 controls energy homeostasis in mice by de novo recruitment of brown adipocytes. Science *328*, 1158-1161.